Norton, K. P., von Blanckenburg, F., Kubik, P. W. (2010): Cosmogenic nuclide-derived rates of diffusive and episodic erosion in the glacially sculpted upper Rhone Valley, Swiss Alps. - Earth Surface Processes and Landforms, 35, 6, 651-662

DOI: 10.1002/esp.1961

Cosmogenic nuclide-derived rates of diffusive and episodic erosion in the glacially sculpted upper Rhone Valley, Swiss Alps

Earth Surface Processes and Landforms (2010), *doi: 10.1002/esp.1961*

Kevin P. Norton[1*], Friedhelm von Blanckenburg[1+] and Peter W. Kubik[2]

[1]Institute for Mineralogy, Leibniz University of Hannover, Germany
[2]Laboratory for Ion Beam Physics, ETH, Zurich, Switzerland

[*]Correspondence to: Kevin P. Norton, Institute for Geology, University of Bern, Switzerland.
E-mail: norton@geo.unibe.ch
[+]Present address: German Research Center for Geosciences GFZ, Potsdam, Germany

ABSTRACT

Denudation rates of small tributary valleys in the upper Rhone valley of the Swiss Central Alps vary by more than an order of magnitude within a very small distance (tens of kilometers). Morphometric data indicate two distinct erosion processes operate in these steep mountain valleys. We determined the rates of these processes using cosmogenic beryllium-10 (^{10}Be) in pooled soil and stream sediment samples. Denudation in deep, glacially scoured valleys is characterized by rapid, non-uniform processes, such as debris flows and rock falls. In these steep valleys denudation rates are 760–2100 mm kyr^{-1}. In those basins which show minimal previous glacial modification denudation rates are low with 60–560 mm kyr^{-1}. The denudation rate in each basin represents a binary mixture between the rapid, non-uniform processes, and soil creep. The soil production rate measured with cosmogenic ^{10}Be in soil samples averages at 60 mm kyr^{-1}. Mixing calculations suggest that the debris flows and rock falls are occurring at rates up to 3000–7000 mm kyr^{-1}. These very high rates occur in the absence of baselevel lowering, since the tributaries drain into the Rhone trunk stream up-stream of a knickzone. The flux-weighted spatial average of denudation rates for the upper Rhone valley is 1400 mm kyr^{-1}, which is similar to rock uplift rates determined in this area from leveling. The pace and location of erosion processes are determined by the oscillation between a glacial and a non-glacial state, preventing the landscape from reaching equilibrium.

KEYWORDS: central Swiss Alps; cosmogenic 10Be; denudation rates

Introduction

Models of orogenic processes suggest that mountains will approach a topographic steady state such that the tectonic mass flux into the mountain belt is balanced by erosional mass flux out of the belt (Whipple *et al.*, 1999; Willett and Brandon, 2002; Willett *et al.*, 2001; Whipple and Mead, 2006). While these models relate the magnitude of rock uplift, defined as the absolute vertical movement of a parcel of rock relative to the stationary geoid or its relative vertical movement with respect to a topographic point of reference, and the associated denudation rate in a purely numeric way, they do not necessarily include a full characterization of the surface processes relating these two fluxes (England and Molnar, 1990; Gilchrist and Summerfield, 1991). Characterization of the underlying processes becomes particularly important during the waning stages of orogenesis when rock uplift and denudation are related solely through isostatic response. This relation is not a straightforward one: uplift and denudation are part of a circular feedback system, where removal of mass from the orogen through denudation promotes rock uplift by means of isostatic adjustment. This rock uplift in turn promotes denudation through steeper slopes and enhanced stream power (Molnarand England, 1990; Whipple, 2001; Wobus *et al.*, 2006). Previous work in the Central European Alps has shown that the denudation rates as measured by cosmogenic beryllium-10 (^{10}Be) in sediment from large rivers (Wittmann *et al.*, 2007; Norton *et al.*, 2008) are balancing the rock uplift rates calculated from leveling over approximately a 100 year timescale (Kahle *et al.*, 1997; Schlatter *et al.*, 2005). Given that modern convergence rates in this part of the Alps are also below the detection limit of a global positioning system (GPS) (Calais *et al.*, 2002), a purely isostatic relation between rock uplift and denudation as suggested in general terms by Molnar and England (1990) is indeed implied. Furthermore, Champagnac *et al.* (2007, 2009) determined that the rock uplift which resulted from erosional unloading during the Quaternary in the Alps accounts for at least 50% of the modern measured rock uplift rates (Kahle *et al.*, 1997; Schlatter *et al.*, 2005), lending support to this interpretation. The purpose of this study is to suggest a process linkage between rock uplift and denudation in isostatically compensated orogens. Such mechanisms are important to understand because; unlike as is the case for a convergent orogen where an

accretionary mass flux is responsible for rock uplift, denudation is the key to continued rock uplift in decaying orogens.

One mechanism often suggested to set the pace of modern denudation in high mountainous settings is the magnitude and frequency of glacial erosion. Repeated Quaternary glaciations have eroded wide, over-steepened valleys (Zhang *et al.*, 2001; Molnar and England, 1990; Small and Anderson, 1998). Even if the magnitude of glacial erosion was not significant during the last cold cycle, the cumulative effect of previous glacial and inter-glacial cycles has been the creation of a landscape that is populated by steep slopes. Such slopes are not sustainable over graded time scales, and as such are transient features in the landscape. These steep hillslopes are the domain of rock falls, landslides and debris flows, while the surrounding lowgradient soil-mantled slopes denude primarily through sediment creep. In this, and indeed any, landscape in which denudation is the result of more than one process, the basinaveraged denudation rate will lie somewhere between that of the slowest and fastest rates in the basin. In terms of instantaneous rates, the lower limit of basin-averaged denudation rates is equal to the rate resulting from diffusive hillslope creep and the maximum theoretical rate is equal to the rate resulting from landslides and debris fl ows. The denudation rate of soil creep is potentially faster than that from shallow landslides. However, if the landslide reoccurrence interval is short, the long-term denudation rate from landslides will also be faster than that for soil creep. The large difference in transport rates between these geomorphic processes should translate into different denudation rates for basins in which the relative importance of creep versus landsliding varies. The central Swiss Alps are a perfect example for such a transient landscape. Here we use a combination of basin-averaged and amalgamated soil denudation rates calculated from new measurements of cosmogenic ^{10}Be to quantify these process rates over various spatial scales. We show that in the upper Rhone valley, denudation rates vary by an order of magnitude, and that episodic processes of mass wasting outweigh hillslope diffusion where glaciers have shaped particularly steep valleys. We further show that the spatially averaged denudation rate is that of the local rock uplift value, even though a bedrock knickzone at the valley outlet hinders baselevel lowering and thereby disconnects the valley from the regional rock uplift trends.

Setting

The upper Rhone Valley, Goms (Figure 1), is located in the Swiss Central Alps between Furka Pass and the town of Fiesch. The sampled basins to the north and south of the Rhone River are underlain by the Aare and Gotthard Massifs respectively. Where it crops out in the Goms, the Aare Massif is composed primarily of foliated gneisses with schists occurring in highly sheared zones. In the northeast, the Aare granite crops out at high elevations. The Gotthard Massif consists of alternating gneisses and schists (Labhart, 1977). Both units are heavily sheared, with shear zones and joints striking nearly parallel to the Rhone River, north-northeast and dipping steeply to the north-northwest to vertical. Sandwiched between the two crystalline units is the meta-sedimentary Furka-Urseren-Garvera Zone and Gomser Zwischenmassif. These rocks are not found in the side valleys and crop out in the main Rhone valley.

Repeated Pleistocene glaciations sculpted the wide U-shaped valley of the upper Rhone valley which was filled with at least 1500 m of ice during the Last Glacial Maximum (LGM) (Jäckli, 1970; Florineth and Schlüchter, 1998; Kelly *et al.*, 2004). The larger valley glaciers of the central three valleys were eroded more extensively than the glaciers in the adjacent valleys, generating exceptionally higher relief. Sequential topographic profiles of the northern valleys parallel to the Rhone show the effects of these glaciations on the lateral tributary valleys in the Goms (Figure 2). Retreat of the LGM Rhone glacier began by 21 kyr $_{BP}$ (Ivy-Ochs *et al.*, 2004). Ice retreated throughout the Alps during the Bølling interstadial; the Rhone Valley was ice free by at least ~15 kyr $_{BP}$ (Welten, 1982; Maisch, 1987) and the surrounding passes were ice free by 14–11 kyr $_{BP}$ (Kelly *et al.*, 2006). The retreat of the Rhone valley glacier left behind hanging tributary valleys which were later incised, forming V-shaped valleys (Figure 2). Throughout the Alps, rivers including the Rhone are incising into LGM surfaces and fills (Schlunegger *et al.*, 2002; Norton *et al.*, 2008) in response to the differential rock uplift and deglaciation. The side valleys are separated by broad soil-mantled ridges. At lower elevations, triangular faceted surfaces are found between the streams (Figure 3a). The side valleys with the highest elevation headwaters were occupied by valley glaciers, lasting till the Younger Dryas. Where these glaciers were large, the valleys have been deeply scoured, with wide valley bottoms, U-shaped cross-sections, and steep walls (Figure 3c). The three scoured valleys, the Minstigerbach, Reckingerbach, and Walibach (which was not sampled) in Figure 1, are still host to small modern glaciers between 0·5 and 3 km2 in size. In all other side valleys, Pleistocene glaciers were either too small to scour the main valleys or non-erosive, leading to cirque basins with post-glacial, fl uvially incised lower reaches (Figure 3b). Upon the retreat of the Rhone glacier, previously active faults or shear zones were reactivated (Ustaszewski and Pfiffner, 2008). As reported by Ustaszewski and Pfiffner (2008) and Persaud and Pfiffner (2004), such post-glacial surface ruptures are common features throughout the Swiss Alps. In most cases, these post-glacial scarps have valley-side-up geometries [e.g. the down-slope side of the fault is upthrown, creating a positive step in the landscape (Figure 3b)]. Individual faults can be followed for up to 4 km. Faults

scarps in the non-glaciated basins in the upper Rhone Valley are continuous from the ridge tops across the valley bottoms and have throws up to 10 m (Ustaszewski and Pfiffner, 2008). In the case of glacially scoured basins, the composite fault scarps are only present on the ridge tops and valley sides, disappearing in the valley bottoms. The faults in the valleys to the south of the Rhone strike more southerly than the main ridge with the result that fewer faults occur in the south-western valleys than in the south-eastern valleys (Figure 1).

Methods

Quantifying the distribution of geomorphic processes was partially accomplished by mapping the occurrence of soil cover, bedrock, rock fall and scree, faults and debris flows (Figure 4a) using a combination of topographic maps, satellite imagery, and field observations. Basin area as well as mean basin elevation and slope were calculated using standard methods in ArcGIS using a 30 m digital elevation dataset. Stream profiles (Figure 5a) were extracted from SwissTopo 25K map sheets Ulrichen and Binntal. Hypsometric curves and hillslope frequency (Figures 5b and 5c) were calculated by extracting elevations and gradients for each basin. The mean hillslope per aspect (Figure 5d) was calculated on a basinwide basis by determining the average hillslope for each aspect direction. The aspects for the southern data were rotated by 180° so that the down-stream directions overlap with those of the northern basins. Rock uplift rates for individual basins were interpolated by splining the existing dataset (Kahle *et al.*, 1997; Schlatter *et al.*, 2005).

We determined *in situ*-produced cosmogenic ^{10}Be derived denudation rates on a total of 35 stream sediments and soils in the upper Rhone valley. Seventeen stream sediment samples, of ~5 kg each, were collected from 15 drainage basins in the Goms (Figure 1). Due to the differing lithologies, the lateral valleys are subdivided into those entering the Rhone from the north (Wilerbach, Hilperschbach, Reckingerbach, Minstigerbach, Geschinerbach, Niderbach, Oberbach, Milibach) and from the south (Ritzibach, Spissbach, Chrimpebach, Bettulbach, Rufi bach, Löümibach). (The sample names used from this point on consist of the first three to five letters of the stream names.) Northern stream samples came from two main settings, glacially scoured valleys with U-shaped cross-sections (Rec, Mins), and fluvially dominated valleys lacking evidence of extensive glacial scouring (Wil, Hil, Ges, Nider, Ober, and Mil). In three valleys, stream sediment was also sampled in the upper part of the basins (Wil2, Hil2, Nider2, and Nider3). Beryllium was extracted from quartz in the 0·125–0·25 mm, 0·25–0·5 mm, or 0·5–1·0 mm grain size fractions. Three main geomorphic surfaces were selected for soil sampling: ridges, valley sides, and interfluvial surfaces (Figure 3a). In order to capture the maximum variability of each region, we adopted a semi-random sampling scheme (e.g. Riebe *et al.*, 2004). A total of 92 soil samples of ~0·5 kg each were combined based on geomorphic location into 18 different amalgamated samples of between four and 12 individual samples, Ober-R, Ober-Rg, Ober-V, Ober-I, Nider-V, Nider-Vg, Mil-R, Mil-V, Bet-R, Bet-V, Hil-R, Hil-I, Wil-R, and Wil-I (Table I). Soil depths were not measured explicitly at each sampling location, however, soil depths of up to 100 cm averaging less than 50 cm were observed in shallow landslide scars, trail cuts, and those soil pits which extended to bedrock. We note that the method of amalgamation, based on equal mass, potentially smoothes the soildenudation rates as slower rates are over-represented. Without prior knowledge of the spatial distribution of denudation rates, however, this method provides the most reliable means of determining denudation rates. Soil samples used the 0·25–0·5 mm size fraction, however for two samples, Hil-I and Ober-R, multiple grain sizes were investigated in order to identify possible particle size infl uences on denudation rate.

^{10}Be was extracted using standard methods (von Blanckenburg *et al.*, 1996; von Blanckenburg *et al.*, 2004), ^{10}Be/^{9}Be ratios were measured in BeO targets prepared by evaporating and oxidizing Be together with $AgNO_3$. Ratio measurements were performed with accelerator mass spectrometry at ETH Zurich as described by Synal *et al.* (1997) relative to the standard S555 using a nominal ^{10}Be/^{9}Be ratio of $95{\cdot}5 \times 10^{-12}$ which is based on a ^{10}Be half-life of 1·51. Approximately 200 μg of ^{9}Be carrier were added to each sample and to blank measurements. Total procedure blanks were determined to contain a ^{10}Be/^{9}Be ratio of $1{\cdot}4 \pm 0{\cdot}5 \times 10^{-14}$. This error was propagated into ^{10}Be concentrations which are presented in Table I at 1σ.

Because this landscape was covered with thick ice up to as recently as 15 kyr $_{BP}$ (Ivy-Ochs *et al.*, 2006), and some of our denudation rates are low, steady state with respect to cosmogenic nuclides can not necessarily be assumed. We therefore used the non-steady state solution of Lal's (1991) equation including production by nucleons, fast muons, and stopped muons (Schaller *et al.* 2002):

$$N(t) = \sum_{i=1}^{8} \frac{P_i(0)}{\lambda + \frac{\rho\varepsilon}{\Lambda_i}} \times \left(1 - e^{-\left(\lambda + \frac{\rho\varepsilon}{\Lambda_i}\right)t} \right) \quad (1)$$

where the concentration of cosmogenic nuclides at the surface, $N(t)$, is governed by both the denudation rate, ε, and the initial exposure age, t. Pi(0) and Λi are the individual polynomial expressions for production rate and

absorption mean free path, respectively for nucleons, fast and stopped muons described in Schaller *et al.* (2002), ρ is rock density (2·7 g cm^{-3}), and λ is the 1·39 ± 0·1 Ma half-life of ^{10}Be (Chmeleff *et al.*, 2009). Scaling followed the latitude and altitude scaling laws of Dunai (2000). Corrections for geomagnetic field variations were not made. The effects of a magnetic field correction on the stream data would be to reduce the denudation rates by no more than 10%. This effect would be negligible for the soils since the correction factor for the 7–15 kyr apparent ages of the soil samples is nearly zero. Topographic shielding factors were calculated on a pixel-by-pixel basis (Norton and Vanacker, 2009) from topographic map sheet-based 30 m digital elevation data (data source: de Ferranti, 2005). Snow shielding factors were calculated using an altitude-dependent snow depth and duration function derived from the monthly Swiss snow depth maps of Auer (2003). In addition to snow shielding, the production rates under the presently glaciated areas were set to zero. Amalgamated soil sample denudation rates were calculated in the same manner, except that shielding factors and production rates were calculated for each sampling point and averaged. Finally, modern landslides in the Goms occur within the thin soil mantled zone. Therefore, the perturbations to denudation rates due to the occurrence of deep-seated landslides should not be a significant factor here (Niemi *et al.*, 2005; Yanites *et al.*, 2009).

Results

Stream profiles and valley cross profiles (Figures 5a and 2, respectively) show that the glaciated basins (Mins, Rec, and Wali) are more deeply incised than the non-glaciated basins. While non-glaciated basins north of the Rhone exhibit relatively linear profiles, those south of the Rhone are strongly convex in the upper reaches and concave in the lower reaches. Basin hypsometries (Figure 5b) for the northern non-glaciated and glaciated basins resemble those suggested by Brocklehurst and Whipple (2004) for cirque glaciation and larger valley glaciers, respectively. The higher hypsometries in the currently non-glaciated basins are the result of minor erosion at high elevations by cirque glaciers which skews the elevation frequency to higher values, and the lower hypsometric integrals for the glaciated basins are due to valley glaciers scouring deeply into the valleys (Brocklehurst and Whipple, 2004). The southern non-glaciated valleys display widely varying hypsometries. Basin hypsometry has been shown to scale with basin area (Hurtrez *et al.*, 1999). The more convex shapes displayed by the non-glaciated basins could also be partially due to basin scaling effects. However, as the ~five-fold difference in the areas of the non-glaciated basins is not accompanied by differences in hypsometry, and the variable hypsometries of the southern non-glacial valley are only weakly correlated with basin area, we suggest that differences in analyzed basin area do not bias our interpretation.

10Be-derived basin-averaged denudation rates in the lateral valleys of the upper Rhone basin vary from 61 to 2100 mm kyr^{-1} (Table I). To the north of the Rhone, the highest rates are found in basins that are currently glaciated in their uppermost parts, while the lowest are found in the non-glacial valleys (Figure 6a). We suggest that the rates from the glacial basins are valid despite the possibility of sediment input from beneath the glacier. Wittmann *et al.* (2007) showed that modern glacial outwash from Alpine glaciers has an average 10Be concentration of ~1500 atoms g$_{qtz}^{-1}$, and a compilation by Hallet *et al.* (1996) reports average glacial erosion rates of 970 mm kyr^{-1} for Alpine glaciers. Using these values together with the background denudation value of 57 mm kyr^{-1} and a nuclide concentration of ~320 000 atoms g$_{qtz}^{-1}$ derived from our soil data, the perturbation to the measured basin-averaged nuclide concentration can be calculated with the formula:

$$N_{mix} = \frac{N_g \varepsilon_g A_g + N_b \varepsilon_b A_b}{\varepsilon_g A_g + \varepsilon_b A_b} \quad (2)$$

where N is the nuclide concentration, ε is the denudation rate, A is the area, and the subscripts g, b, and mix stand for glacial, background, and mixed, respectively. For our basins, the nuclide concentrations decrease at the most by 20% as calculated for the Minstigerbach. The resulting concentration would result in a maximum denudation rate of ~200 mm ky^{-1} due solely to mixing with subglacial sediments. As this value is ten-fold slower than the measured value (see Table 1), we interpret the fast denudation rates in the glacial basins to be due to surface erosion and not to glacial perturbation. In the southern valleys, where there is no evidence of Holocene glacial cover, a wide range of denudation rates from 240-1400 mm ky^{-1} were also measured. For the valleys in which upper-basin samples were also taken (Nider2, Nider3, Wil2, Hil2), the rates are always similar to those measured near the confluence with the Rhone.

Denudation rates calculated from pooled-soil samples are comparatively quite homogeneous, with rates varying from 22-99 mm ky^{-1} (Figure 7a, Table 1). Grain size replicates for O-R and H-I show that there is no dependence of soil denudation rate on grain size for the size fractions used in this study. Based on the apparent ages of 1-15 ky, denudation rates average over the entire post-glacial period for all but the fastest-eroding basins. Because of the long averaging times, the effects of intense historic human modification are unlikely to significantly affect the cosmogenic nuclide budget in this setting (von Blanckenburg, 2005). We consider these soil denudation rates to be equivalent to soil production rates. This is a valid assumption if soil production and erosion have continued

sufficiently long enough to reach steady state. Based on a minimum time since glaciation of 15ky, an average soil depth of ~0.5 m and an average soil denudation rate of 57 mm ky^{-1}, the entire soil column would have been exchanged between once and twice, supporting the case for steady state between soil production at depth and soil removal through denudation (both chemical and physical weathering). These soil production rates are also similar to soil production rates of ~4 to 160 mm ky^{-1} when scaled to a density of 2.7 mm ky^{-1} reported by Heimsath et al. (1997; 2000; 2001) at the saprolite-bedrock boundary for similar lithologies in the western USA and Australia.

Despite the uniformity of denudation rates, some geomorphic information can be gleaned from the amalgamated soils. We exclude the 4 sample locations underlain by granite from this part of the analysis in order to avoid a bias based on lithology, as the granitic samples consistently have lower denudation rates than the samples from the gneissic lithologies. The landform with the lowest hillslope gradients are the ridges at 24º, which also have the lowest average denudation rates with 30-64 mm ky^{-1}, while the valley slopes, with slopes of 28º, have higher average denudation rates of ~62-99 mm ky^{-1}. The triangular facet samples at the steepest angle of 34° denude at intermediate rates of 51-77 mm ky^{-1}. Our data further show that slowly denuding soil-mantled slopes can be maintained at very high hillslope gradients (Figure 6, Table 1). That the triangular faceted surfaces have lower denudation rates than the valley hillslopes despite higher gradients is contradictory to previous studies (Ahnert, 1970; Montgomery and Brandon, 2002). This is probably due to forest cover which is common at these lower elevations, but absent in the higher valley slopes. The presence of deeper-rooting vegetation might also explain how these steep terrains are able to sustain soil cover at all. These triangular facets are, however, prone to very low frequency large-scale deep seated failure as is evidenced by the presence of large landslide-debris flow scars on some of the interfluves (e.g. Figure 3a).

Based on field mapping and aerial imagery, the percentage of soil-covered slopes in the northern valleys is between 43 and 87% (Figure 4a, Table 2). Bedrock exposure varies between 0 and 28%, with blocky debris and glaciers making up the remaining surface area. Using the amalgamated soil denudation rates as the rate of hillslope creep together with the total basin averaged denudation rates, an area-weighted estimate of the effect of mixing frequent, rapid, stochastic, transport processes (i.e. rock falls, debris flows, etc.) on the entire area can be calculated. We tested both soil cover and bedrock cover (Figure 8), with bedrock correlating best with denudation rate, $R^2 = 0.90$ (Figure 8b). From the mixing line shown in Figure 8b, an end member denudation rate of roughly 7600 mm ky^{-1} can be inferred. The value based on the correlation with soil cover ($R^2 = 0.80$; Figure 8a) provides a more conservative estimate of ~3000 mm ky^{-1} for the non-soil mantled end member. That there is a difference between the 0% soil and 100% bedrock denudation rate end member calculations suggests that the system is more complicated than a simple bimodal distribution, however, it is clear that the zones sourcing debris flows and rock falls do have an order of magnitude higher overall rate than those zones experiencing only soil creep. These estimates are subject to large uncertainty due in part to the narrow grain size range investigated here. Many authors (Brown et al., 1995; 1998; Belmont et al., 2008; Niemi et al., 2005) have suggested that stochastic processes such as the large-scale rockfalls and debris flows produce different grain size distributions and potentially different cosmogenic nuclide concentrations than in creep-dominated landscapes (Yanites et al., 2009). However, the large difference between the denudation rates recorded for the landslide dominated basins vs. the soil creep dominated basins suggests that our grain size fractions do include this signal. This observation suggests that the rapid, stochastic processes in the Central Alps are generating fine-grained material.

Discussion

Denudation processes and rates

A comparison of soil denudation rates which range from 22 to 99 mm ky^{-1} and basin-averaged denudation rates of 61 to 2100 mm ky^{-1} reveal a decidedly non-uniform erosional pattern. Basin-averaged denudation rates from river sediments draining northern valleys are up to 100 times those of amalgamated soil denudation rate values. We suggest that this is due to varying degrees of mixing between the two dominant modes of denudation that are common in the upper Rhone Valley. Basins with extensive soil mantling are dominated by diffusive creep, while high frequency stochastic processes (rock falls, landslides, and debris flows) are prevalent where soils are lacking. Furthermore, when plotted against mean basin slope, the basin-averaged denudation rates show the non-linear increase that is expected (e.g. Roering et al., 1999, 2007; Montgomery and Brandon, 2000, Binnie et al., 2007) while the pooled-soil rates remain low even at high slope angles (Figure 6). Landscape denudation rates are commonly interpreted with reference to threshold hillslopes Burbank et al., 1996; Montgomery and Brandon 2002; Binnie et al., 2007). Two types of gradients are commonly discussed; critical slopes and threshold slopes. The critical slope, S_c as introduced by Roering et al. (1999; 2001), is equal to 0.56 to 1.25 m m^{-1} or ~30-50° and is a maximum ideal hillslope. At the critical slope, the rate of sediment transport is infinitely high, and further hillslope steepening becomes impossible. Therefore, the critical slope should in practice never be attained in the landscape. However, one requirement of the critical slope concept is that transportable sediment is always available on the hillslopes. When settings are weathering-limited, such that soil is erosion is limited by the rate at which it is produced, slopes higher than the critical slope are allowable. The threshold hillslope is typically

defined as the slope at which linear and non-linear creep processes give way to stochastic landsliding. Using an analog model, Roering et al. (2001) showed that for cohesive sediments, this transition occurs at a gradient of 0.48 (~26°) for a critical slope of 0.56 (~30°). Burbank et al., 1996 suggested that the mean slope angle is controlled by bedrock fracturing, placing the threshold transition near 32° in the Himalaya as measured with the 90 m SRTM dataset. Similarly, Montgomery and Brandon (2002) showed that erosion rates in the Olympic Mountains become non-correlated with gradient above slopes of ~30°. Here we model the denudation rates in the Goms with the same erosion law;

$$E = E_0 + \frac{KS}{1 - \frac{S}{S_c}} \tag{3}$$

where E is the modeled erosion rate, E_0 is the background erosion rate of 57 mm ky^{-1} (our soil production rate), K is an erosion constant, S the mean basin slope and S_c the critical slope. The best fit to the data (Figure 6) yield a critical slope of ~33°. The presence of slopes steeper than the critical slope in the upper Rhone valley suggests that at least a portion of these hillslopes are in a supply-limited state in which sediment production does not keep pace with denudation. The modeled erosion constant of 200 mm ky^{-1} is half that of the Olympic Mountains, indicating that erosion rates increase more slowly with slope in this setting. The threshold transition from creep to a domain dominated by landsliding occurs above the non-linear portion of the curve at ~30° (Figure 6). We interpret this to be the threshold hillslope angle for the upper Rhone Valley. This value is also supported by the results of the geomorphic mapping. The mean slope of the soil-mantled regions is 26 degrees, while debris flow channels and exposed bedrock are associated with slopes of 33° and 35° respectively. The steepest slopes in the Goms are associated with a lack of soil cover. The frequency distribution of hillslopes shows a potential genetic difference between the basin types. While the modal value of hillslopes in the northern non-glaciated basins lies below the threshold gradient, those for the glaciated and southern basins are above the threshold gradient. Above 30°, the northern glaciated and southern basins have a higher frequency of hillslopes (Figure 5c) than the non-glaciated basins. The distribution of hillslope angle with aspect (Figure 5d) shows that many of the higher slopes in the glaciated basins are associated with slopes that face up-stream (e.g. away from the Rhone Valley). These steep slopes are located in the areas with the highest hillslope relief (Figure 4b) and coincide with the locations of debris flow channels in the glaciated basins (Figure 4a).

The highest denudation rates in the northern basins are associated with the largest drainage areas, presence of glaciers, high relief, abundant exposed bedrock, number of debris flows, and a lack of cross-valley obstructions (e.g. valley-side-up faults). While this makes it difficult to attribute variations in denudation rate to any one of these causes, it is not unexpected as most of these parameters are tightly interrelated. The larger glaciers (and interglacial streams) of the central 3 basins incised more deeply during the Pleistocene than did the smaller adjacent glaciers (and streams). This is the primary cause for the higher relief in the glaciated basins (e.g. Whipple et al., 1999). It is precisely these zones of high relief, generated by glacial erosion, in which abundant bedrock outcrops and debris flow channels are located. There, faults and other linear features such as shear and jointing zones, act to focus sediment down the hillslopes, creating debris flow channels (Figures 4a and 5d).

The hillslopes adjacent to the main stream channels have much higher relief in the glacial valleys than in the non-glacial valleys. Roering et al. (2001) showed experimentally that once these hillslopes pass beyond the threshold gradient for hillslope creep, the system will switch to one in which landsliding prevails. Indeed, in the glaciated basins, the steep valley walls erode through landsliding and debris flow action. Creep, however, is still the main denudational process on the soil-mantled hillslopes between the debris flow channels (Figure 3c). The result is that the relative contribution of creep to the sum of all erosion processes is much lower than that of the non-glacial valleys.

The southern basins have widely variable hypsometric curves (Figure 5b. The south-easternmost valleys feature hypsometric curves very similar to those of the non-glacial northern valleys, while the westernmost basins have nearly linear hypsometric curves indicating more immature watersheds. This gradient in hypsometric parameters can be explained with an additional forcing mechanism to which the southern basins are subject which varies either in time or space. Due to the presence of a migrating knickzone at the outlet of the upper Rhone valley, the western-most of these valleys are actively adjusting to a rapidly dropping baselevel (Figure 7b). This spatial gradient can be treated as a temporal gradient as well. As the knickzone migrates to the northeast the basins are sequentially impacted, with less modification in the Ritzibach and Spissbach basins and more modification in the Rufibach and Löümibach basins. Denudation rates also decrease from 1000-1400 mm ky^{-1} in the southwest to ~200 mm ky^{-1} in the northeast. In this sense, these basins offer a glimpse into the processes which create these side valleys. Initial depressions in the hillside, such as the large scale landslide and debris flow scars located on the interfluvial surfaces (e.g. Figure 3a), are destabilized by fluvial baselevel lowering. These basins in turn react by deeply incising through debris flow processes, as is currently occurring in the Rufibach, until the stream profile approaches that of a steady-state stream.

Rock uplift and denudation rates

The upper Rhone valley is subject to some of the highest rates of rock uplift in the Swiss Alps (Kahle et al., 1997; Schlatter et al., 2005), varying from 700 mm ky^{-1} at the northeastern end to 1300 mm ky^{-1}at the southwestern end relative to a benchmark at Aarburg in the Swiss foreland. Wittmann et al. (2007) showed that denudation rates for the Alps are correlated with rock uplift rates, suggesting that in the Goms, where uplift rates range between 700 and 1300 mm ky^{-1}, a NE-SW gradient of denudation rates from around 800 to 1400 mm ky^{-1} would be expected, which is not the case (Figure 9). The probable cause for the absence of this correlation is the presence of a bedrock knickzone near the southwest end of the valley. Because the uplift rates increase in a downstream direction, the knickzone acts as a barrier to the Alpine-wide baselevel lowering. The rock uplift rate at the knickzone is ~1200 mm ky^{-1}. By recalculating the rock uplift rates of the upper Rhone valley relative to their local baselevel (e.g. subtracting the rate at the knickzone from those upstream), zero to negative rock uplift rates (e.g. subsidence) can be inferred (Figure 7a). In this case, rock uplift is neither lowering the relative base level, nor steepening streams. The connection between rock uplift and denudation should at least in part be through differential uplift driven changes in base levels (Whipple, 2001; Wobus et al., 2006). In the Goms, streams are decoupled from high regional rock uplift rates. Without this geomorphic connection between rock uplift and denudation through river incision, an alternative explanation for the large variation in denudation rates of the lateral valleys in the Goms is needed. We suggest the variations are dependent on the spatial distribution of soil-mantled slopes versus bedrock, which in turn is related to the efficacy of glacial erosion throughout the Quaternary.

The southern basins support the interpretation of a disconnection between rock uplift rates and denudation rates in the upper Rhone valley. Unlike the northern basins, which are all located upstream of the bedrock knickpoint, the southern basins extend into the knickzone. Those basins which are upstream of the knickzone have denudation rates which are similar to those of the non-glaciated northern basins; however the basins which are within the broad knickzone have elevated denudation rates of 760 to 1400 mm ky^{-1}, which is in the range predicted by the relationship presented by Wittmann et al. (2007).

Interestingly, an area- and flux-weighted denudation rate for all the tributaries studied here results in a denudation rate of 1400 mm ky^{-1} for the entire upper Goms valley. This rate is similar to large-catchment rates in this part of the Central Alps (Wittmann et al., 2007) and also within the range of geodetic rock uplift rates (Kahle et al., 1997; Schlatter et al., 2005). We observe that the specific relative spatial occurrence of rapid and slow erosional processes in the upper Rhone valley set the rate of denudation. This process takes place in the absence of possible uplift-driven base level lowering in the form of bedrock incision in the Rhone trunk stream; lending support to the hypothesis that denudation, resulting from glacially steepened landscapes may be setting the pace of rock uplift in the Central Alps.

CONCLUSIONS

We have shown that pre-conditioning by glacial erosion during the Pleistocene has created an oversteepened landscape in the Goms in which rock fall and debris flows can accelerate basin-averaged denudation rates through increased spatial occurrence. It is possible to quantify the effects of geomorphic history on surface denudation by combining ^{10}Be derived basin-averaged and pooled-soil denudation rates. Soil-mantled hillslopes denude at a "background" rate of 22-99 mm ky^{-1}, controlled by the soil production rate. Based on a mixing analysis, debris flows and rock falls overwhelm the denudational system with erosion rates of up to 7600 mm ky^{-1}, where the conditions prevail for these types of mass wasting. These high denudation rates occur despite being located upstream of a prominent bedrock knickzone at the valley outlet. The knickzone causes the upper Rhone valley to be detached from the largest of the baselevel fluctuations and rock uplift rates that have affected the post-LGM Alps. We suggest that the glacial erosion that is responsible for oversteepening slopes, thereby providing a means through which high erosion rates can exist in an area which, due to the effect of a bedrock knickzone, has low local relative rock uplift rates. Yet, the combination of all denudation processes results in a mean Rhone Valley-wide denudation rate of 1400 mm ky^{-1}, which is similar to the rock uplift rate in this area relative to the benchmark in the northern foreland. Therefore, despite being in a geomorphic sense, detached from the regional rock uplift pattern, the significant relief generated in the glaciated basins of the Goms provides a feedback mechanism coupling denudation at the valley scale with regional rock uplift rates. The implication is that relief generation by Quaternary glaciation is capable of driving both local denudation processes and regional-scale rock uplift.

ACKNOWLEDGMENTS

The authors would like to thank Jen Dahl for the illustration in Figure 3. Veerle Vanacker and Hella Wittmann were of much help in the field, and Sabine Schwienbacher helped with sample preparation. We would also like to thank the participants of the European Surface Process Group 2008 fieldtrip for in depth discussions on this topic. We are particularly indebted to Steve Binnie, Isaac Larsen, and two anonymous reviewers for thoughtful and thorough comments.

REFERENCES CITED

Ahnert F. 1970. Functional relationship between denudation, relief, and uplift in large mid-latitude drainage basins. *American Journal of Science* **268**: 243-263.

Auer M. 2003. Regionalisierung von Schneeparametern - eine Methode zur darstellung von Schneeparametern im Relief. Unpublished Master's Thesis. Universität Bern: 97 pp.

Belmont P, Pazzaglia FJ, and Gosse JC. 2007. Cosmogenic ^{10}Be as a tracer for hillslope and channel sediment dynamics in the Clearwater River, western Washington State. *Earth and Planetary Science Letters* **264**: 123-135.

Binnie S, Phillips W, Summerfield MA, Fifield LK. 2007. Tectonic uplift, threshold hillslopes, and denudation rates in a developing mountain range. *Geology* **35**:743-746.

Brocklehurst SH, Whipple KX, 2004. Hypsometry of glaciated landscapes. *Earth Surface Processes and Landforms* **29**: 907-926.

Brown ET, Stallard RF, Larsen MC, Bourles DL, Raisbeck GM and Yiou F. 1998. Determination of predevelopment denudation rates of an agricultural watershed (Cayaguas River, Puerto Rico) using in-situ-produced ^{10}Be in river-borne quartz. *Earth and Planetary Science Letters* **160**: 723-728.

Brown ET, Stallard RF, Larsen MC, Raisbeck GM and Yiou F. 1995. Denudation rates determined from the accumulation of in situ- produced ^{10}Be in the Luquillo experimental forest, Puerto Rico. *Earth and Planetary Science Letters* **129**: 193-202.

Burbank DW, Leleand J, Fielding E, Anderson RS, Brozovic N, Reid MR, Duncan C. 1996. Bedrock incision, rock uplift and threshold hillslopes in the northwestern Himalayas. *Nature* **379**: 505-510.

Calais E, Nocquet J, Jouanne F, and Tardy M. 2002. Current strain regime in the Western Alps from continuous Global Positioning System measurements, 1996-2001. *Geology* **30**: 651-654.

Champagnac J, Molnar P, Anderson R, Sue C, Delacou B. 2007. Quaternary erosion-induced isostatic rebound in the Western Alps. *Geology* **35**: 195-198.

Chmeleff J, von Blanckenburg F, Kossert K, Jakob D. 2009. Determination of the ^{10}Be half-life by Multi Collector ICP-Mass Spectrometry and Liquid Scintillation Counting. *Goldschmidt Conference Davos, Geochimica et Cosmochimica Acta* **73**: A221.

de Ferranti, J. 1“ resolution digital elevation data for the European Alps. http://www.viewfinderpanoramas.org/dem3.html

Dunai T. 2000. Scaling factors for production rates of in situ produced cosmogenic nuclides: a critical reevaluation. *Earth and Planetary Science Letters* **176**: 157-169.

England P, Molnar P. 1990. Surface uplift, uplift of rocks, and exhumation of rocks. *Geology* **18**: 1173-1177.

Florineth D, Schlüchter C. 1998. Reconstructing the Last Glacial Maximum (LGM) ice surface geometry and flowlines in the Central Swiss Alps. *Eclogae Geologicae Helvetiae* **91**: 391-407.

Gilchrist AR, Summerfield MA. 1991. Denudation, isostasy and landscape evolution. *Earth Surface Processes and Landforms* **16**: 555-562.

Hallet B, Hunter L, Bogen J. 1996. Rates of erosion and sediment evacuation by glaciers: A review of field data and their implications. *Global and Planetary Change* **12**: 213-235.

Heimsath A, Dietrich W, Nishiizumi K, Finkel R. 1997. The soil production function and landscape equilibrium. *Nature* **388**: 358-361.

Heimsath A, Chappell J, Dietrich W, Nishiizumi K, Finkel R. 2000. Soil production on a retreating escarpment in southeastern Australia. *Geology* **28**: 787-790.

Heimsath A, Dietrich W, Nishiizumi K, Finkel R. 2001. Stochastic processes of soil production and transport: erosion rates, topographic variation and cosmogenic nuclides in the Oregon Coast Range. *Earth Surface Processes and Landforms* **26**: 531-552.

Ivy-Ochs S, Schaefer J, Kubik P, Synal H, Schlüchter C. 2004. Timing of deglaciation on the northern Alpine Foreland (Switzerland). *Eclogae Geologicae Helvetiae* **97**: 47-55.

Jäckli A. 1970. Die Schweiz zur letzten Eiszeit. In Atlas der Schweiz. Bundesamt für Landestopographie (Ed.). Wabern-Bern.

Kahle H, Geiger A, Buerki B, Gubler E, Marti U, Wirth B, Rothacher M, Gurtner W, Beutler G, Bauersima I, and Pfiffner OA. 1997. Recent crustal movements, geoid and density distribution: contribution from integrated satellite and terrestrial measurements. In *Results of the national research program 20 (NRP 20).* Pfiffner OEA (Ed.): 251-259.

Kelly M, Buoncristiani J, Schlüchter C. 2004. A reconstruction of the Last Glacial Maximum (LGM) ice-surface geometry in the Western Swiss Alps and contiguous alpine regions in Italy and France. *Eclogae Geologicae Helvetiae* **97**: 57-75.

Kelly M, Ivy-Ochs S, Kubik P, von Blanckenburg F, Schlüchter C. 2006. Chronology of deglaciation based on ^{10}Be dates of glacial erosional features in the Grimsel Pass region, Central Swiss Alps. *Boreas* **35**: 634-643.

Lal D. 1991. Cosmic ray labeling of erosion surfaces: in situ nuclide production rates and erosion models. *Earth and Planetary Science Letters* **104**: 424-439.

Labhart TP. 1977. Aarmassiv und Gotthardmassiv. *Samllung Geolischer Fuehrer* **63**. Borntraeger Berlin-Stuttgart, Germany: 173 pg.
Maisch M. 1987. Zur Gletscher- und Klimageschichte des alpinen Spätglazials: Analyse und Interpretation von Schneegrenzdaten. *Geographica Helvetica* **42**: 63-71.
Molnar P, England P. 1990. Late Cenozoic uplift of mountain ranges and global climate change: chicken or egg?. *Nature* **346**: 29-34.
Montgomery D. 2001. Slope distributions, threshold hillslopes, and steady-state topography. *American Journal of Science* **301**: 432-454.
Montgomery D, Brandon M. 2002. Topographic controls on erosion rates in tectonically active mountain ranges. *Earth and Planetary Science Letters* **201**: 481-489.
Niemi N, Oskin M, Burbank D, Heimsath A, Gabet E. 2005. Effects of bedrock landslides on cosmogenically determined erosion rates. *Earth and Planetary Science Letters* **237**: 480-498.
Norton KP, Vanacker V. 2009. Effects of terrain smoothing on topographic shielding correction factors for cosmogenic nuclide-derived estimates of basin-averaged denudation rates. *Earth Surface Processes and Landforms* **34**: 145-154. DOI: 10.1002/esp.1700.
Norton KP, von Blanckenburg F, Schlunegger F, Schwab M, Kubik PW. 2008. Cosmogenic nuclide-based investigation of spatial erosion and hillslope channel coupling in the transient foreland of the Swiss Alps. *Geomorphology* **95**: 474-486. doi:10.1016/j.geomorph.2007.07.013
Persaud M, Pfiffner OA. 2004. Active deformation in the Eastern Swiss Alps: post-glacial faults, seismicity and surface uplift. *Tectonophysics* **385**: 59-84.
Riebe C, Kirchner JW, Finkel R. 2004. Sharp decrease in long-term chemical weathering rates along an altitudinal transect. *Earth and Planetary Science Letters* **218**: 421-434.
Roering JJ, Kirchner JW, Dietrich W. 1999. Evidence for nonlinear, diffusive sediment transport on hillslopes and implications for landscape morphology. *Water Resources Research* **35**: 853-870.
Roering JJ, Kirchner JW, Sklar LS, Dietrich WE. 2001. Hillslope evolution by nonlinear creep and landsliding: An experimental study. *Geology* **29**: 143-146.
Roering JJ, Peron JT, Kirchner JW. 2007. Functional relationships between denudation and hillslope form and relief. *Earth and Planetary Science Letters* **264**: 245-258.
Schaller M, von Blanckenburg F, Veldkamp A, Tebbens L, Hovius N, Kubik PK. 2002. A 30000 yr record of erosion rates from cosmogenic ^{10}Be in middle European river terraces. *Earth and Planetary Science Letters* **204**: 307-320.
Schlatter A, Schneider D, Geiger A, Kahle H. 2005. Recent vertical movements from precise levelling in the vicinity of the city of Basel, Switzerland. *International Journal of Earth Sciences (Geologische Rundschau)* **94**: 507-514.
Small EE, Anderson RS. 1998. Pleistocene relief production in Laramide mountain ranges, western United States. *Geology* **26**: 123-126.
Synal H, Bonani G, Doebeli M, Ender R, Gartenmann P, Kubik PK, Schnabel C, Suter M. 1997. Status report of the PSI/ETH AMS facility. *Nuclear Instruments and Methods in Physics Research, Section B: Beam Interactions with Materials and Atoms* **B123**: 62-68.
Ustaszewski M, Pfiffner OA. 2008. Neotectonic faulting, uplift and seismicity in the central and western Swiss Alps. In: Siegesmund, S., Fügenschuh, B., Froitzheim, N. (eds.). *Tectonic Aspects of the Alpine-Dinaride-Carpathian System*. Geological Society, London, **Special Publications 298**: 231-249. DOI: 10.1144/SP298.12.
von Blanckenburg F. 2005. The control mechanisms of erosion and weathering at basin scale from cosmogenic nuclides in river sediment. *Earth and Planetary Science Letters* **237**: 462-479.
von Blanckenburg F, Belshaw N, O´Nions RK. 1996. Separation of Be-9 and cosmogenic Be-10 from environmental materials and SIMS isotope dilution analysis. *Chemical Geology*. **129**: 93-99.
von Blanckenburg F, Hewawasam T, Kubik PW. 2004. Cosmogenic nuclide evidence for low weathering and denudation in the wet, tropical highlands of Sri Lanka. *Journal of Geophysical Research*. **109**: F03008, doi03010.01029/02003JF000049
Welten, M, 1982, Vegetationsgeschichtliche Untersuchungen in den westlichen Schweizer Alpen; Bern-Wallis. *Denkschriften der Schweizerischen Naturforschenden Gesellschaft* **95**: 1-105.
Whipple KX ,Mead BJ. 2006. Orogen response to changes in climatic and tectonic forcing. *Earth and Planetary Science Letters* **243**: 218-228.
Whipple KX, Kirby E, Brockelhurst SH. 1999. Geomorphic limits to climate-induced increases in topographic relief. *Nature* **401**: 39-41.
Whipple KX. 2001. Fluvial landscape response time: How plausible is steady-state denudation? *American Journal of Science* **301**: 313-325.
Willett SD, Brandon MT. 2002. On steady states in mountain belts. *Geology* **30**: 175-178.

Wittmann H, von Blanckenburg F, Kruesmann T, Norton KP, Kubik PW. 2007. The relation between rock uplift and denudation from cosmogenic nuclides in river sediment in the Central Alps of Switzerland. *Journal of Geophysical Research A: Earth Surface* **112**: F04010.

Wobus C, Whipple KX, Kirby E, Snyder N, Johnson J, Spyropolou K, Crosby B, Sheehan D. 2006. Tectonics from topography: Procedures, promise, and pitfalls, *in* Willet SD; Hovius N; Brandon MT; Fisher DM *eds.*, Tectonics, Climate, and Landscape Evolution: *GSA Special Paper* **398**: 57-74.

Yanites BJ, Tucker GE, Anderson RS. 2009. Numerical and analytical models of cosmogenic radionuclide dynamics in landslide-dominated drainage basins. *Journal of Geophysical Research* **114**, F01007, doi:10.1029/2008JF001088,

Zhang P, Molnar P, Downs W. 2001. Increased sedimentation rates and grain sizes 2-4 Myr ago due to the influence of climate change on erosion rates. *Nature* **410**: 891-897.

Figures

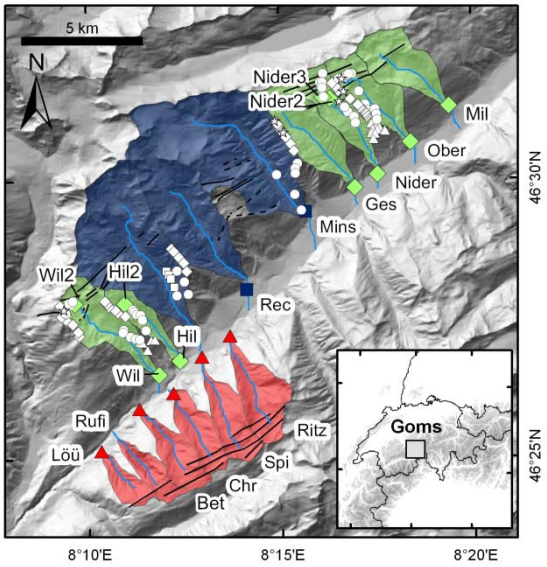

Figure 1: Location map showing stream sample locations (glacially scoured basins indicated by squares, non-glaciated basins by diamonds and southern basins by triangles). Soil sample locations are shown in white (ridge top with a diamond, valley side with a star, triangular faceted surface with a triangle). Photograph locations for Figure 3 are marked with arrows. This figure is available in colour online at www.interscience.wiley.com/journal/espl

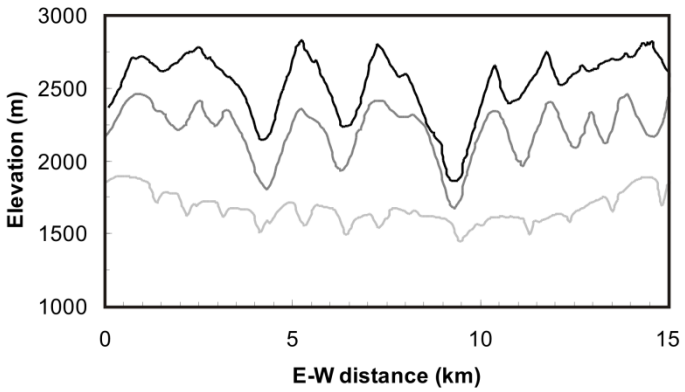

Figure 2: Topographic profiles of the northern side of the Rhone valley, running parallel to the Rhone at distances of 1 km (light grey), 2·5 km (medium grey), and 4 km (black) from the river (see Figure 4b for locations). The 2·5 km and 4 km profiles show that over 500 m more relief has been generated in the glaciated basins (three central valleys) versus the non-glaciated basins. The extra relief is not apparent for the 1 km profi le because all the lateral streams are near the local baselevel (Rhone).

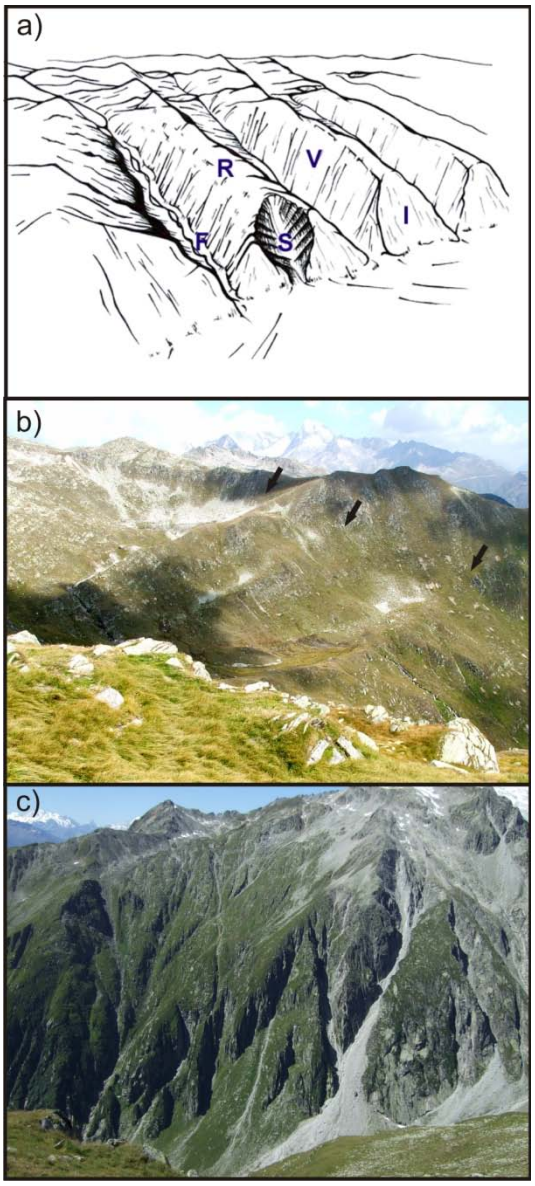

Figure 3: (a) Schematic diagram of the lateral valleys of the Goms, showing; ridges (R), valleys (V), triangular faceted surfaces (I), colluvial fans (F), and large-scale failure scars (S).
(b) The upper sections of the Oberbach basin, where valley-side-up scarps are indicated by arrows.
(c) In the Minsterbach, where glaciers have generated steep valley sides with alternating debris flows and soil mantled slopes. This figure is available in colour online at www.interscience.wiley.com/journal/espl

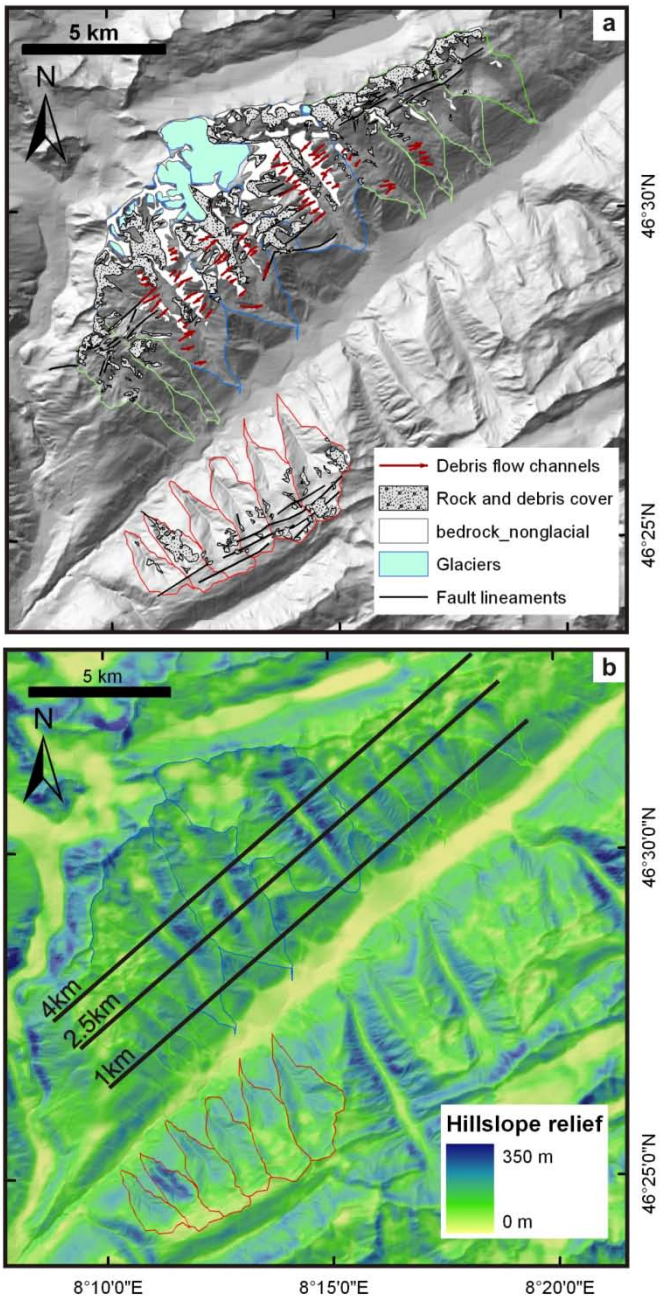

Figure 4: Shaded relief map from 30 m digital elevation data of the study area showing
(a) dominant surface cover type,
(b) relief based on a 240 m sliding window. This length scale corresponds to the smallest hillslope lengths in order to obtain maximum hillslope relief measurements. The surface cover map is derived from areal photographs, topographic maps, and field mapping and shows the locations of valley-side-up fault scarps and debris flow channels as well as glaciers, blocky debris, and bedrock. Note that the remaining areas without symbols are soil mantled. The lines denote the trace of the topographic profiles at 4, 2·5, and 1 km distance from the Rhone main stream as shown in Figure 2. This figure is available in colour online at www.interscience.wiley.com/journal/espl

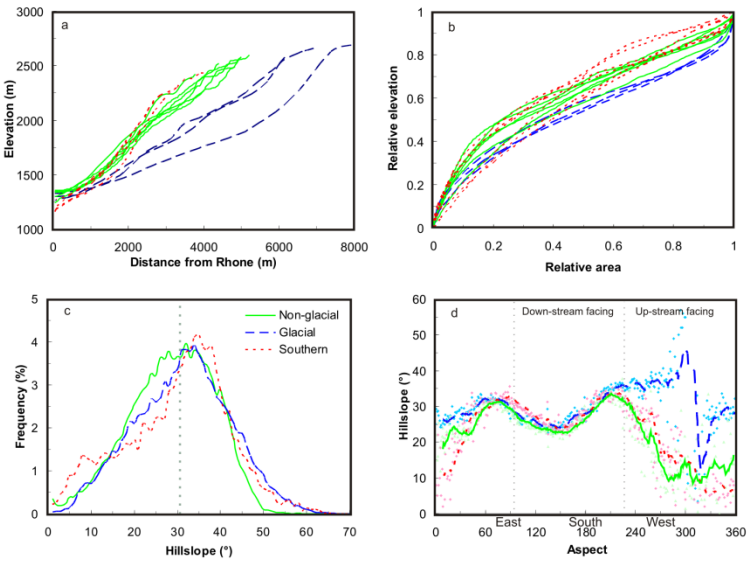

Figure 5: Topographic metrics for the studied basins. In all cases, northern glaciated basins are shown by the long dashed lines, northern nonglaciated basins by the joined lines, and southern non-glaciated basins by the dotted lines.
(a) Stream profiles extracted from SwissTopo 1:25 000 maps (Ulrichen and Binntal).
(b) Hypsometric curves for each basin.
(c) Averaged hillsope frequency for each region, the local threshold hillslope angle, ~33° (dashed line) derived from Figure 6 is also shown.
(d) Average hillslope angle for each hillslope aspect (note that the southern data have been rotated by 180° for direct comparison). This figure is available in colour online at www.interscience.wiley.com/journal/espl

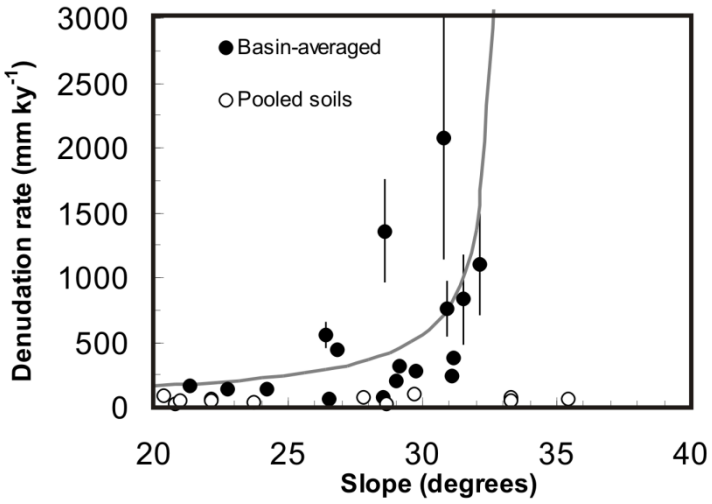

Figure 6: (a) Basin-averaged denudation rates for the Goms watersheds. The *x*-axis is the southwest-northeast (SW-NE) location of the valleys along the Rhone River. Glacially scoured basins (squares) to the north of the Rhone have considerably higher denudation rates than non-glaciated basins (diamonds). To the south of the Rhone (triangles) denudation rates increase towards the southwest. Amalgamated soil samples (open symbols match those in Figure 1) are consistently low. Three measured rock uplift rates are shown at their leveling site within the valley (Schlatter *et al.*, 2005) by grey diamonds (with one standard deviation error bars) with the interpolated values are shown by a solid grey line. Rock uplift rates relative to a stable knickzone are shown by the grey dashed line.
(b) Stream profiles for the Rhone River (black) and the side valleys of the Goms (long dashed lines, joined lines and dotted lines) with elevation demarked on the right *y*-axis. The bedrock knickzone is shown by shading. This figure is available in colour online at www.interscience.wiley.com/journal/espl

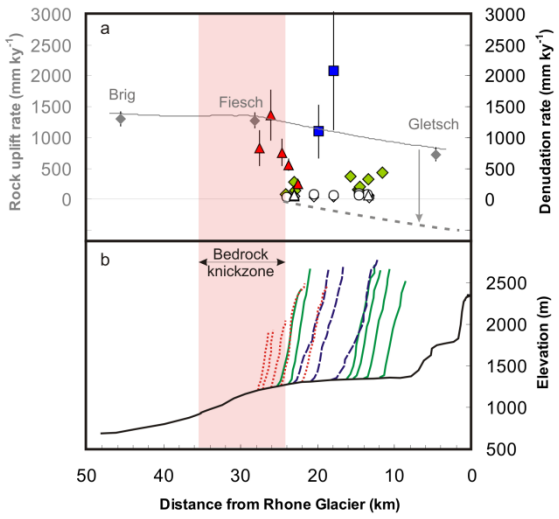

Figure 7: Denudation rates plotted against mean hillslope for both basin-averaged sediment samples (filled circles) and amalgamated soil samples (open circles). Basin-averaged denudation rates are limited at threshold hillslope angles, with rates increasing dramatically above ~30°. We model the denudation rates with the formulation of Montgomery and Brandon (2002) (equation 3), using a K value of 200 mm yr^{-1}, a background erosion rate of 57 mm kyr^{-1} (our average soil denudation rate) and a critical slope of ~33° (grey line). Denudation rates from amalgamated soil samples show no correlation with hillslope gradients, remaining between ~80 and 150 mm kyr^{-1} regardless of slope. Mean hillslope angle for the basin-averaged samples is the mean-basin slope. For the soil samples, mean hillslope angles are the average of the hillslopes for the sampling locations. In both cases, the values are calculated from the 30 m digital elevation dataset, and therefore represent minimum values.

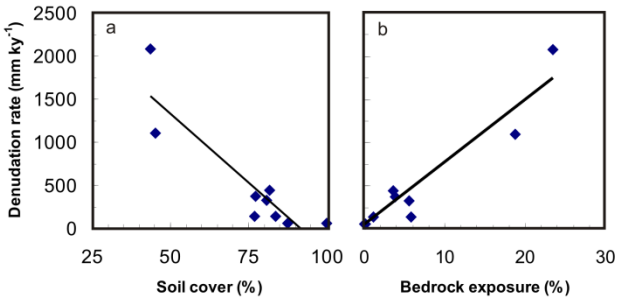

Figure 8: Relationship between basin-averaged denudation rate and
(a) percent soil cover for each drainage basin (R^2 = 0·83) and
(b) percent exposed bedrock (R^2 = 0·89). While the trends are partially dependent on extreme data values, a significant correlation exists in both cases ($R2$ = 0·31 and 0·40 respectively) even if these points are excluded.

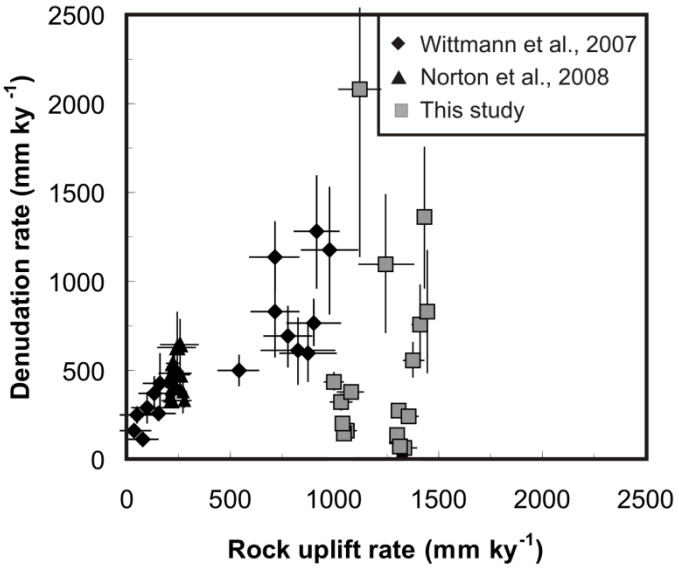

Figure 9: Relationship between denudation rate and rock uplift rate for the Central Alps (Wittmann *et al.*, 2007), Alpine Foreland (Norton *et al.*, 2008) and this study with one standard deviation error bars. Rock uplift rates for the Goms drainage basins were estimated by interpolating between the three nearest uplift stations (Schlatter *et al.*, 2005).

Table 1. Topographic and cosmogenic nuclide data. The second term in the soil names refers to the geomorphic domain; R for ridge, V for valley, and I for triangular facet. The postscript "g" is included for granite parent rock; all other soils are developed on gneissic rocks.

	Sample [a]	Longitude [b] (dd)	Latitude [b] (dd)	Area [c] (km^2)	Slope [c] (degrees)	Altitude [c] (m)	^{10}Be conc. (10^4 atoms g_{qtz}^{-1})	Shielding factor [d]	Snow factor [d]	Denudation rate [e] (steady state) (mm ky^{-1})	Denudation rate [f] (15kyr) (mm ky^{-1})	Aparent age [g] (ky)
Streams	Mil	8.3230	46.5223	4.1	27	2355	4.14 ± 0.44	0.95	0.84	466 ± 53	439 ± 52	1.5
	Ober	8.3061	46.5115	3.6	29	2302	5.44 ± 0.69	0.95	0.84	345 ± 48	321 ± 46	2.0
	Nider1	8.2692	46.5246	0.9	21	2687	13.4 ± 1.3	0.97	0.81	174 ± 17	159 ± 17	3.9
	Nider2	8.2723	46.5243	1.09	23	2686	14.59 ± 0.99	0.97	0.81	160 ± 11	144 ± 11	4.3
	Nider3	8.2921	46.5011	2.9	29	2312	8.63 ± 0.96	0.94	0.84	218 ± 25	199 ± 25	3.2
	Ges	8.2814	46.4994	9.5	31	2335	4.67 ± 0.47	0.94	0.83	402 ± 43	377 ± 41	1.7
	Mins	8.2608	46.4908	14.6	31	2492	0.74 ± 0.19	0.92	0.62	2120 ± 960	2080 ± 940	0.33
	Rec	8.2392	46.4681	12.2	32	2517	1.58 ± 0.39	0.92	0.70	1130 ± 440	1100 ± 390	0.61
	Hil	8.2081	46.4477	1.6	30	2142	5.78 ± 0.58	0.94	0.85	297 ± 32	273 ± 31	2.4
	Hil2	8.1826	46.4631	0.3	24	2513	14.0 ± 1.3	0.97	0.82	152 ± 15	135 ± 14	4.5
	Wil	8.1971	46.4424	4.9	27	2379	23.3 ± 1.5	0.95	0.83	84 ± 5.7	60.5 ± 7.8	8.2
	Wil2	8.1731	46.4594	0.4	29	2632	23.3 ± 1.7	0.96	0.81	97 ± 7.5	76.2 ± 8.9	7.1
	Ritz	8.2257	46.4520	4.1	31	2147	6.45 ± 0.91	0.93	0.85	264 ± 42	242 ± 38	2.7
	Spi	8.2107	46.4464	2.8	26	2219	3.04 ± 0.48	0.95	0.85	591 ± 100	560 ± 100	1.2
	Chr	8.2038	46.4362	2.7	31	2032	2.01 ± 0.42	0.94	0.86	800 ± 220	760 ± 220	0.89
	Bet	8.1886	46.4315	2.3	29	2082	1.18 ± 0.25	0.94	0.86	1410 ± 410	1370 ± 400	0.50
	Lou	8.1722	46.4185	1.4	32	1927	1.72 ± 0.41	0.94	0.87	880 ± 290	830 ± 350	0.82
Soils	O-R	8.287	46.522	-	22	2659	28.68 ± 0.88	0.99	0.81	86.9 ± 2.7	64.1 ± 2.7	7.9
	O-R(2)	8.287	46.522	-	22	2349	26.0 ± 1.4	0.99	0.84	80.0 ± 4.4	53.9 ± 4.4	8.7
	O-Rg	8.278	46.529	-	29	2623	43.0 ± 1.7	0.98	0.81	56.2 ± 2.2	21.8 ± 2.2	12
	O-Vg	8.279	46.534	-	20	2631	22.9 ± 1.6	0.98	0.81	106.6 ± 7.9	87.2 ± 7.9	6.4
	O-I	8.295	46.515	-	35	2029	19.0 ± 1.4	0.96	0.86	88.2 ± 7.0	62.0 ± 7.0	8.1
	N-V	8.281	46.522	-	30	2164	15.1 ± 1.5	0.96	0.85	120 ± 12	99 ± 12	5.9
	N-Vg	8.268	46.529	-	24	2637	35.4 ± 1.8	0.98	0.81	68.5 ± 3.7	40.1 ± 3.7	10
	H-R	8.176	46.466	-	21	2573	38.1 ± 1.3	0.98	0.82	61.5 ± 2.0	29.7 ± 2.0	11
	H-I	8.195	46.453	-	33	1867	16.3 ± 1.5	0.96	0.87	92.8 ± 9.2	66.3 ± 9.2	7.8
	H-I(2)	8.195	46.453	-	33	1867	14.9 ± 1.1	0.96	0.87	102.1 ± 7.8	76.9 ± 7.8	7.1
	H-I(3)	8.195	46.453	-	33	1867	18.87 ± 0.81	0.96	0.87	80.0 ± 3.5	50.9 ± 3.5	9.0
	W-R	8.159	46.459	-	21	2659	31.4 ± 2.6	0.99	0.81	79.4 ± 6.9	54.7 ± 6.9	8.6
	W-V	8.177	46.471	-	28	2403	22.3 ± 1.8	0.96	0.83	93.5 ± 7.7	70.9 ± 7.7	7.4
	M-V	8.257	46.501	-	33	1910	16.62 ± 1.50	0.92	0.87	89 ± 12	62 ± 12	8.1
	M-Rg	8.256	46.512	-	32	2641	39.12 ± 3.25	0.98	0.81	62.2 ± 9.0	31.1 ± 9.0	11
	M-R	8.253	46.515	-	18	2519	34.16 ± 1.84	0.99	0.82	67.1 ± 8.2	37.6 ± 8.2	10
	B-V	8.209	46.469	-	31	1967	15.96 ± 1.12	0.95	0.87	99 ± 12	75 ± 12	7.2
	B-R	8.207	46.479	-	26	2415	32.10 ± 1.17	0.98	0.83	66.6 ± 7.7	36.4 ± 7.7	10

[a] All samples are 0.25-0.5 mm except if otherwise noted. b = 0.125-0.25 mm, c = 0.5-1.0 mm

[b] As they are amalgamated, the soil sample locations are approximate.

[c] Topographic metrics were calculated from the 30" SRTM database.

[d] Topographic shielding was calculated from the SRTM database following Norton and Vanacker (2009) and snow shielding corrections are based on annual Swiss snow data (Auer, 2002).

[e] Denudation rate calculations based on the scaling laws of Dunai (2000) and production equations of Schaller et al. (2002) assuming cosmogenic stready state.

[f] Denudation rate calculations based on the scaling laws of Dunai (2000) and production equations of Schaller et al. (2002) assuming an initial exposure age of 15 ky.

[g] Apparent ages are calculated assuming cosmogenic steady state.

Table 2. Percent surface cover characteristics.

	% bedrock	% debris	% glaciers	% soil
Mil	4	14	0	82
Ober	6	14	0	81
Nider	6	17	0	77
Ges	4	18	1	77
Mins	23	15	18	43
Rec	19	21	15	45
Wali	28	17	4	51
Hil	1	15	0	84
Wil	0	13	0	87
Ritz	3	15	0	82
Spi	2	9	0	89
Chr	0	4	0	96
Bet	0	6	0	94
Rufi	0	32	0	68
Lou	0	3	0	97